Catalase−Peroxidase Active Site Restructuring by a Distant and "Inactive" Domain†

Ruletha D. Baker,‡ Carma O. Cook,‡ and Douglas C. Goodwin*

Department of Chemistry and Biochemistry, Auburn University, Auburn, Alabama 36849-5312

Received November 22, 2005; Revised Manuscript Received April 18, 2006

ABSTRACT: Catalase−peroxidases are composed of two peroxidase-like domains. The N-terminal domain contains the heme-dependent, bifunctional active site. The C-terminal domain does not bind heme, has no catalytic activity, and is separated from the active site by >30 Å. Nevertheless, without the C-terminal domain, the N-terminal domain exhibits neither catalase nor peroxidase activity due to the apparent coordination of the distal histidine to the heme iron. Here we report the ability of the separately expressed and isolated C-terminal domain ($KatG^C$) to restructure the N-terminal domain ($KatG^N$) to its bifunctional conformation. Addition of equimolar $KatG^C$ to $KatG^N$ decreased the hexacoordinate low-spin heme complex and increased the high-spin species (pentacoordinate and hexacoordinate). EPR spectra of the domain mixture showed a distribution between high-spin species nearly identical to that of wild-type KatG. The CD spectrum for the 1:1 physical mixture of the domains was identical to an arithmetic composite of individual spectra for $KatG^N$ and $KatG^C$. Both physical and arithmetic mixtures were nearly identical to the spectrum for wild-type KatG, suggesting that major shifts in secondary structure did not accompany active site reconfiguration. With the shift in heme environment, the parallel return of catalase *and* peroxidase activity was observed. Inclusion of bovine serum albumin instead of $KatG^C$ produced no activity, indicating that specific interdomain interactions were required to reestablish the bifunctional active site. Apparent constants for reactivation ($k_{react} \sim 4 \times 10^{-3}$ min^{-1}) indicate that a slow process like movement of established structural elements may precede the restructuring of the heme environment and return of catalytic activity.

Catalase−peroxidases have a single multifunctional active site that facilitates efficient catalase *and* peroxidase activities. These enzymes have generated considerable biomedical interest. Catalase−peroxidase (KatG)[1] from *Mycobacterium tuberculosis* has been exploited for the activation of the front-line antitubercular agent isoniazid to its antibiotic form. Interestingly, the increasing prevelance of isoniazid-resistant *M. tuberculosis* is strongly tied (over 70% of resistant strains) to mutations that compromise the ability of KatG to catalyze activation (*3*). It is also interesting to note that a novel group of periplasmic catalase−peroxidases have been identified as potential virulence factors in dangerous pathogens such as the enterohemorrhagic *Escherichia coli* strain O157:H7 (*4*) and *Yersinia pestis* (*5*−*7*), both of which are recognized as high priority threats as agents of bioterrorism. Nevertheless, the mechanisms by which these enzymes may operate as virulence factors have not been illuminated. Clearly, there are important benefits to be derived from understanding the structure and function of the catalase−peroxidases.

The disproportionation of H_2O_2 (i.e., catalase activity) by heme-dependent catalases, including the catalase−peroxidases, starts with reaction of resting enzyme with 1 equiv of H_2O_2 to yield H_2O and an oxoferryl porphyrin/protein radical intermediate (compound **I**) (Scheme 1). Compound **I** is then reduced back to resting enzyme by a second equivalent of H_2O_2, generating O_2 and H_2O. The peroxidase catalytic cycle also begins with compound **I** formation. However, compound **I** is reduced in two sequential one-electron steps by an exogenous electron donor to return the enzyme to its ferric state. The first reduction produces 1 equiv of substrate radical and, with typical peroxidases (e.g., horseradish peroxidase), the oxoferryl intermediate known as compound **II**. However, recent evidence suggests that in catalase−peroxidases the heme iron is reduced first to yield an Fe^{III}−OH/protein radical complex (*8*). In both cases, the second reductive step produces the resting enzyme and a second equivalent of substrate radical.

Though these two catalytic processes are similar, the bifunctional ability of the catalase−peroxidases is highly unusual. Heme enzymes with substantial catalase activity typically exhibit poor peroxidase activity. Likewise, the heme enzymes known for their strong peroxidase activity show very weak catalase activity. The lack of catalase activity in typical peroxidases (e.g., cytochrome *c* peroxidase) is noteworthy because, with few exceptions (*9*), the active sites of these enzymes and the catalase−peroxidases are virtually superimposable on one another (*1*, *10*). This striking

† Funds to support this research were provided by the Petroleum Research Fund of the American Chemical Society (PRF 38802-G4) and Auburn University. C.O.C. is supported by an NSF-Alabama Louis Stokes Alliance for Minority Participation "Bridge to the Doctorate" Research Fellowship.

* To whom correspondence should be addressed. Phone: (334) 844-6992. Fax: (334) 844-6959. E-mail: goodwdc@auburn.edu.

‡ R.D.B. and C.O.C. contributed equally to the execution and description of this research.

[1] Abbreviations: KatG, *Escherichia coli* catalase−peroxidase; wt-KatG, wild-type KatG; $KatG^N$, KatG N-terminal domain; $KatG^C$, KatG C-terminal domain; MnP, manganese peroxidase; LiP, lignin peroxidase; ABTS, 2,2′-azinobis(3-ethylbenzothiazoline-6-sulfonic acid); IPTG, isopropyl β-D-thiogalactopyranoside; Ni-NTA, nickel nitrilotriacetate; LB broth, Luria−Bertani broth; δ-ALA, δ-aminolevulinic acid; PMSF, phenylmethanesulfonyl fluoride.

10.1021/bi052392y CCC: $33.50
Published on Web 05/17/2006

Scheme 1: Representation of the Dual Catalytic Cycle of Catalase−Peroxidases[a]

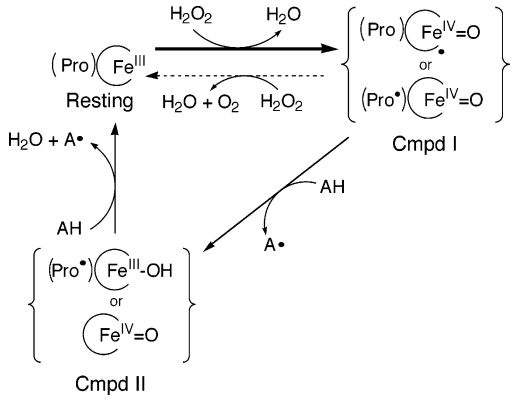

[a] Catalase activity involves cycling between the resting and compound I (Cmpd I) forms. Peroxidase activity includes the reactions involving compound II (Cmpd II).

functional difference between two enzymes that are so structurally similar provides a robust system for unraveling the subtle perturbations of heme enzyme active sites that lead to profound differences in mechanism and function.

Along these lines, catalase−peroxidases have three prominent structural features that are absent from monofunctional peroxidases. All three structures are peripheral to the enzyme active site, and evidence suggests that all three are essential for catalase−peroxidase function (*1*, *2*, *10*, *11*). One of these features is a 300 amino acid C-terminal domain. The C-terminal domain also structurally resembles a monofunctional peroxidase, suggesting that its presence in the catalase−peroxidases is due to an ancient gene-duplication event; however, this domain does not bind heme and does not catalyze any discernible reaction. Nevertheless, we have shown that this "inactive" domain is essential for catalase−peroxidase catalysis (*11*). A catalase−peroxidase variant containing only its N-terminal domain ($KatG^N$) lacks catalase *and* peroxidase activities (*11*). Results of site-directed mutagenesis and spectroscopic studies indicate that, in the absence of the C-terminal domain, an active site histidine (the so-called distal histidine) acts as a ligand to the heme iron, interrupting its ability to act as a general base in catalase−peroxidase catalysis.

Here we demonstrate the ability of the separately expressed and isolated C-terminal domain ($KatG^C$) to restructure the active site found within the N-terminal domain ($KatG^N$). Addition of equimolar $KatG^C$ to $KatG^N$ resulted in a shift in the active site heme coordination environment. There was a decrease in the inactive hexacoordinate low-spin heme typical of $KatG^N$ and a concomitant increase in the high-spin species typical of wild-type catalase−peroxidases. Consistent with these alterations in active site structure, both catalase *and* peroxidase activities were detected. A generic protein, bovine serum albumin, was unable to restore either catalase or peroxidase activities when it was incubated with $KatG^N$ in place of $KatG^C$, indicating that specific interdomain interactions were required for $KatG^N$ activation.

MATERIALS AND METHODS

Materials. Hydrogen peroxide (30%), imidazole, phenyl-Sepharose resin, ampicillin, chloramphenicol, phenylmethanesulfonyl fluoride (PMSF), and 2,2′-azinobis(3-ethylbenzothiazoline-6-sulfonic acid) (ABTS) were purchased from Sigma (St. Louis, MO). Isopropyl β-D-thiogalactopyranoside (IPTG), urea, and tetracycline hydrochloride were obtained from Fisher (Pittsburgh, PA). All restriction enzymes were purchased from New England Biolabs (Beverly, MA), and all oligonucleotide primers were purchased from Invitrogen (Carlsbad, CA). All *E. coli* strains [BL-21(DE3) pLysS and XL-1 Blue] and Pfu polymerase were obtained from Stratagene (La Jolla, CA). Nickel nitrilotriacetic acid (Ni-NTA resin) was obtained from Qiagen (Valencia, CA). All buffers and media were prepared using water purified through a Millipore Q-PakII system (18.2 MΩ/cm resistivity).

Expression and Purification of wtKatG. Expression and purification of wtKatG were carried out as previously described (*2*) except that KatG was eluted from the Ni-NTA column by a linear gradient ranging from buffer A (50 mM phosphate, pH 8.0, 200 mM NaCl) supplemented with 2 mM imidazole to buffer A supplemented with 100 mM imidazole. Imidazole was removed by gel filtration (Sephacryl 300 HR). Appropriate fractions, as determined by SDS−PAGE and catalase assays, were combined and concentrated by ultrafiltration (30000 MW cutoff) and stored at −80 °C.

Expression and Purification of the KatG Domains, $KatG^N$ and $KatG^C$. Expression of the KatG variants was carried out as described for wtKatG except that expression cultures were not supplemented with δ-aminolevulinic acid or ferrous ammonium sulfate.

For $KatG^C$, cell pellets were resuspended in 200 mM phosphate buffer, pH 7.0, supplemented with lysozyme (0.1 mg/mL) and PMSF (0.1 mM). Following homogenization, the suspension was sonicated with a Branson 250 sonifier at constant output, 3.5 duty, for eight cycles consisting of 45 s on and 45 s off. Following sonication, benzonase (500 units) was added to the cell lysate, and the mixture was incubated at room temperature with gentle stirring for 1 h. The cell lysate was then centrifuged at 12000 rpm for 20 min. The pellet was discarded, and the supernatant was loaded onto a Ni-NTA column that had been previously rinsed with 100 mM Tris buffer by recirculating the solution through the column bed overnight at 1 mL/min. The column was then washed with buffer A (200 mM phosphate buffer, pH 7.0). Two sequential washes were then performed with buffer A supplemented with 2 and 20 mM imidazole, respectively. $KatG^C$ was eluted from the column using buffer A supplemented with 200 mM imidazole. Fractions containing $KatG^C$ were combined, and excess imidazole was removed by dialysis (36 h; five buffer changes).

$KatG^N$ was expressed in inclusion bodies. Because of this, following the centrifugation of the lysate, the supernatant was discarded, and the pellet was resuspended in 8 M urea, rehomogenized, and recentrifuged. After the second centrifugation, Ni-NTA resin was added to the supernatant, and the resultant mixture was incubated overnight at 23 °C with constant, gentle agitation. The Ni-NTA resin was then collected on a column and washed with 10 column volumes of 10 mM imidazole in 8 M urea. The target protein was then eluted from the column using 8 M urea supplemented with 200 mM imidazole. The purity of each fraction was estimated by Coomassie-stained SDS−PAGE, and the appropriate fractions (≥95% pure) were pooled and dialyzed against buffer A for 24 h with five changes. The resulting

$KatG^N$ was then reconstituted with 0.95 equiv of hemin and stored at 4 °C.

Domain Mixing and Incubation Procedures. The concentrations of $KatG^N$ and $KatG^C$ were calculated using the molar absorptivities below. Solutions containing $KatG^N$ and $KatG^C$ were incubated at 4 °C for times ranging from 0 to 72 h. Reactivation was also measured as a function of pH. In each case, $KatG^N$ and $KatG^C$ were incubated in the presence of 120 mM buffer (citrate or phosphate) at the appropriate pH. Following a given incubation time, aliquots were removed, and activity was measured according to the assays described below. Assay conditions were such that the added aliquot volume did not significantly affect the pH of the assay. Apparent rate constants for reactivation (k_{react}) as a function of pH were fit to eq 1, where *a* and *b* are the theoretical maximum and minimum k_{react} values, respectively.

$$y = a + (b - a)/(1 + 10^{pK_a - pH}) \quad (1)$$

Catalase and Peroxidase Activity Assays. Peroxidase activity was evaluated by monitoring the production of the ABTS radical over time at 417 nm (34.7 mM^{-1} cm^{-1}) (*12*). All assays were carried out at room temperature in 50 mM acetate buffer, pH 5.0. Catalase activity was evaluated by monitoring the decrease in H_2O_2 concentration with time at 240 nm (39.4 M^{-1} cm^{-1}) (*13*). All assays were carried out at room temperature in 100 mM phosphate buffer, pH 7.0. All catalase and peroxidase activities were normalized on the basis of heme content.

UV−Visible Absorption Spectroscopy. All UV−visible absorption spectra were recorded using a Shimadzu UV1601 spectrophotometer (Columbia, MD). The molar absorptivities of $KatG^N$ (prior to heme addition) and $KatG^C$ at 280 nm were estimated according to the method of Gill and von Hippel (*14*): $\epsilon_{280}(KatG^N) = 1.11 \times 10^5$ M^{-1} cm^{-1} and $\epsilon_{280}(KatG^C) = 3.36 \times 10^4$ M^{-1} cm^{-1}. Concentrations of holo-wtKatG and holo-$KatG^N$ were determined on the basis of the molar absorptivity of the Soret band λ_{max}: ϵ_{408}(wtKatG) $= 1.21 \times 10^5$ M^{-1} cm^{-1} (*2*) and $\epsilon_{416}(KatG^N) = 9.8 \times 10^4$ M^{-1} cm^{-1} (*11*).

Circular Dichroism Spectropolarimetry. Far-UV (185−300 nm) circular dichroism (CD) spectra were recorded for wtKatG, $KatG^N$, $KatG^C$, and a 1:1 mixture of $KatG^N$ and $KatG^C$ using a Jasco J-810 spectropolarimeter (Tokyo, Japan). To minimize buffer interference at wavelengths below 200 nm, all spectra were recorded using 10 mM phosphate buffer, pH 7.0, and Suprasil quartz cells (0.1 mm path length). All spectra were recorded at 23 °C.

Electron Paramagnetic Resonance Spectroscopy. Spectra were recorded using a Bruker EMX instrument equipped with an Oxford ESR 900 cryostat and ITC temperature controller. Additional sample concentration, if necessary, was performed using Amicon Ultra-4 centrifugal filter devices (Beverly, MA). The settings for the spectrometer were as follows: temperature, 10 K; microwave frequency, 9.38 GHz; microwave power, 0.1 mW; modulation amplitude, 10 G; modulation frequency, 100 kHz; time constant, 655.36 ms; conversion time, 655.36 ms; and receiver gain, 1.0×10^5.

RESULTS

To gain additional insight into the role of the C-terminal domain in KatG structure and catalysis, we measured the response of $KatG^N$ to the separately expressed and isolated C-terminal domain ($KatG^C$). Far-UV CD spectra for $KatG^N$ (Figure 1, trace a) and $KatG^C$ (trace b) indicate secondary structural content substantially different from each other and wild-type KatG (trace c). However, a CD spectrum for the physical mixture of $KatG^N$ and $KatG^C$ (1:1 ratio) (trace d) was highly similar to that of wtKatG. The composite spectrum derived arithmetically from the separate spectra for $KatG^N$ and $KatG^C$ was superimposable on the spectrum obtained from the physical mixture of the domains (Figure 1 inset). These data suggest that (1) preparation of the separated domains, $KatG^N$ and $KatG^C$, does not result in major disruption of secondary structural content from that which is expected for each domain from the wild-type enzyme and (2) the physical mixture of $KatG^N$ and $KatG^C$ did not appreciably change the secondary structural content of either protein.

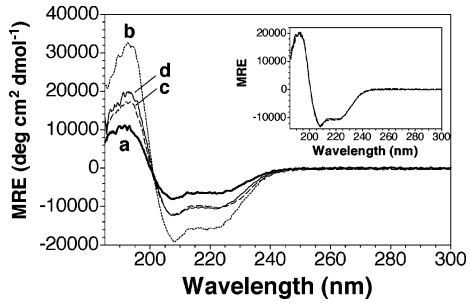

FIGURE 1: Far-UV circular dichroism spectra for wtKatG and each of its separately expressed and isolated domains. Spectra were recorded for $KatG^N$ (a, bold line), $KatG^C$ (b, dotted line), wtKatG (c, dashed line), and an equimolar mixture of $KatG^N$ and $KatG^C$ (d, solid line). The inset shows a comparison of the equimolar mixture of $KatG^N$ and $KatG^C$ to the composite spectrum derived arithmetically from the individual spectra for $KatG^N$ and $KatG^C$. All data are reported in terms of mean residue ellipticity (MRE). The concentration of each protein was 4.3 μM. All spectra were recorded at 23 °C using 10 mM phosphate buffer, pH 7.0.

An equimolar mixture of $KatG^N$ and $KatG^C$ had appreciable catalase and peroxidase activities (Figure 2). Individually, neither $KatG^N$ nor $KatG^C$ had either catalase or peroxidase activity. Furthermore, incubation of $KatG^N$ with a generic protein such as bovine serum albumin (BSA) did not restore either catalase or peroxidase activity, indicating that specific interactions between the domains were essential for restoration of the catalase−peroxidase active site in $KatG^N$.

Further examination revealed that catalase and peroxidase activities increased with time of coincubation of the two domains (Figure 3). At 4 °C, increases in peroxidase and catalase activities were observed over the first 20 h. Interestingly, both activities were observed to return at similar rates. Fits of the observed data to a single exponential equation produced rate constants for reactivation (k_{react}) of 3.4×10^{-3} and 2.5×10^{-3} min^{-1} for catalase and peroxidase activities, respectively.

We measured steady-state kinetic parameters for the catalase activity of the equimolar mixture of $KatG^N$ and $KatG^C$ following 30 min, 24 h, and 48 h incubations at 4 °C (Table 1). These data show that the increase in activity over time (see Figure 3) was due primarily to an effect on the apparent k_{cat}, increasing from roughly 90 s^{-1} following a 30 min incubation with $KatG^C$ to about 2000 s^{-1} following 24 and 48 h incubations. The latter values represent 20% of

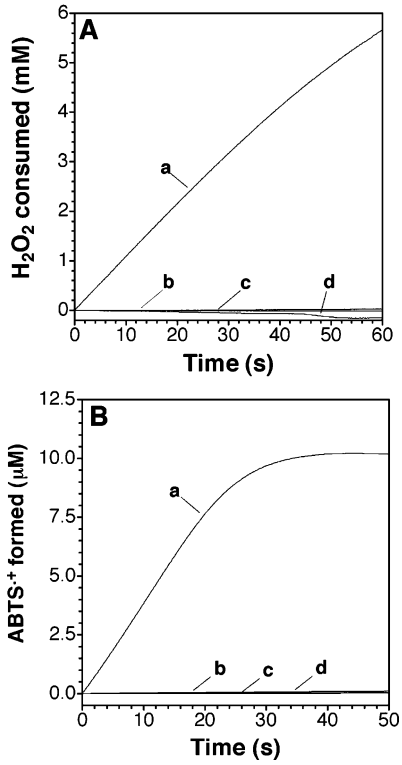

FIGURE 2: Reactivation of $KatG^N$ in the presence of $KatG^C$. Catalase (A) and peroxidase (B) activities were measured for an equimolar mixture of $KatG^N$ and $KatG^C$ (a), $KatG^N$ alone (b), $KatG^C$ alone (c), and an equimolar mixture of $KatG^N$ and bovine serum albumin (d). Catalase activity was measured for a 100 nM concentration of each protein in the presence of 10 mM H_2O_2 and 100 mM phosphate buffer, pH 7.0. Peroxidase activity was measured for a 50 nM concentration of each protein in the presence of 1 mM H_2O_2, 1 mM ABTS, and 50 mM acetate buffer, pH 5.0. All assays were carried out at 23 °C.

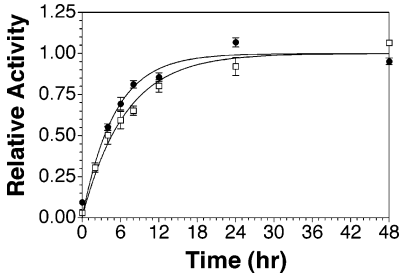

FIGURE 3: Catalase and peroxidase activities over time for an equimolar mixture of $KatG^N$ and $KatG^C$. An equimolar mixture of $KatG^N$ and $KatG^C$ was incubated at 4 °C for an increasing length of time prior to measurement of its catalase (closed circles) and peroxidase (open squares) activities. All activity assays were carried out as described for Figure 2.

those obtained by our laboratory for wild-type KatG (*2*, *15*) and fall between 15% and 60% of the values obtained for catalase−peroxidases from other organisms. Incubation with $KatG^C$ showed relatively little effect on the apparent K_M for H_2O_2. A value of about 2.5 mM was observed following all three coincubation times. This is very similar to the apparent K_M of wild-type KatG for H_2O_2 (*2*, *15*, *16*) and well within the range for that observed for other catalase−peroxidases. The apparent second-order rate constant obtained for the recovered catalase activity was about 9×10^5 M^{-1} s^{-1}.

Likewise, we evaluated the steady-state peroxidase activity of the coincubated domains as a function of H_2O_2. The peroxidase kinetics for wild-type KatG and our $KatG^N/KatG^C$ mixture were complex. Nevertheless, the maximum peroxidase activity (the apparent k_{cat}) followed a trend similar to that determined for catalase activity (Table 1). Following 24 and 48 h incubations with $KatG^C$, values of about 13 s^{-1} were determined and represent about 22% of the value that we have recorded for wild-type KatG (*2*, *15*).

The effect of pH on the rate of $KatG^N$ reactivation by $KatG^C$ was also explored (Figure 4, closed symbols). As the pH decreased from 8.0, there was a progressive increase in the apparent rate constant (k_{react}) for reactivation. The maximum observed k_{react} (9.4×10^{-3} min^{-1}) was obtained at pH 6.0, representing a 7-fold increase in rate. A fit of the data (pH 8−6) to eq 1 yielded an apparent pK_a of 6.2 and predicted a maximum k_{react} of 1.4×10^{-2} min^{-1}. However, below pH 6.0 there was an abrupt decrease in k_{react}, precluding a more complete data set to directly observe the true maximum and more accurately determine the pK_a. Nevertheless, the data suggest 6.5 as an upper limit for the apparent pK_a governing the reactivation of $KatG^N$ by $KatG^C$.

In a similar manner, the extent of reactivation was determined from the amplitudes of the single exponential data obtained at each pH. The amplitude remained essentially constant from pH 8 to at least pH 6.5. Furthermore, in a trend resembling k_{react}, there was an abrupt decrease in amplitude at low pH. The parallel and dramatic disruption of rate and extent of activation suggests that, at low pH, the structural integrity of the free $KatG^N$ or $KatG^C$ may be compromised. Along these lines, we have observed by UV−vis an increased propensity of $KatG^N$ toward unfolding and aggregation at low pH. Within error, k_{react} and amplitude values obtained in the presence of phosphate or citrate buffers were the same, indicating that the behavior at low pH was not due to the buffer itself.

Visible absorption spectra corresponding to the α, *β*, and charge transfer transitions for $KatG^N$ changed little immediately following the addition of an equimolar concentration of the C-terminal domain (Figure 5). However, following a 48 h incubation at 4 °C, increases in absorption corresponding to the short- and long-wavelength charge transfer transitions (near 500 and 645 nm, respectively) were observed. Decreases in the intensities of the α and *β* transitions (536 and 568 nm, respectively) were also observed, and a 4 nm blue shift in the Soret (*γ*) band from 416 to 412 nm was also detected (data not shown). These spectral shifts are all consistent with a loss of the hexacoordinate low-spin heme iron typical of $KatG^N$ along with increases in the high-spin species (hexacoordinate and pentacoordinate) that are typically observed for wild-type KatG. Comparison of the spectrum obtained at 48 h to those of wild-type KatG and $KatG^N$ alone suggests that approximately 50% of the $KatG^N$ has undergone active site restructuring in the presence of $KatG^C$.

In the absence of the $KatG^C$, the EPR spectrum of $KatG^N$ is dominated by signals consistent with a hexacoordinate low-spin heme complex (Figure 6, spectrum a). Indeed, the g_1 (2.92), g_2 (2.28), and g_3 (1.53) values obtained from the spectrum suggest that the strong-field sixth ligand in the coordination sphere is a histidine residue (*17*, *18*). Previous work from this laboratory strongly suggests that this histidine is the so-called distal histidine within the active site of catalase−peroxidases (*11*). Addition of an equimolar con-

Table 1: Apparent Kinetic Parameters for Catalase and Peroxidase Activities from Coincubated $KatG^N$ and $KatG^C$

	catalase[a]			peroxidase[b]
	k_{cat} (s^{-1})	K_M (mM)	k_{cat}/K_M ($M^{-1}\,s^{-1}$)	k_{cat} (s^{-1})
wtKatG[c]	$1.2 \pm 0.2 \times 10^4$	4.0 ± 0.4	$3.1 \pm 0.5 \times 10^6$	58 ± 3
N + C (0.5)[d]	86 ± 18	3.1 ± 0.8	$2.9 \pm 0.3 \times 10^4$	$8 \pm 5 \times 10^{-3}$
N + C (24)	2270 ± 18	2.2 ± 0.2	$1.0 \pm 0.1 \times 10^6$	13 ± 1
N + C (48)	1900 ± 160	2.2 ± 0.1	$8.7 \pm 0.6 \times 10^5$	14 ± 1

[a] Catalase assays included 50 nM $KatG^N$, 50 nM $KatG^C$, and 100 mM phosphate, pH 7.0, 23 °C. [b] Peroxidase assays included 20 nM $KatG^N$, 20 nM $KatG^C$, and 50 mM acetate, pH 5.0, 23 °C. [c] From ref *2*. [d] $KatG^N$ and $KatG^C$ (1:1) incubated at 4 °C in 120 mM phosphate, pH 7.0, for *x* hours (in parentheses).

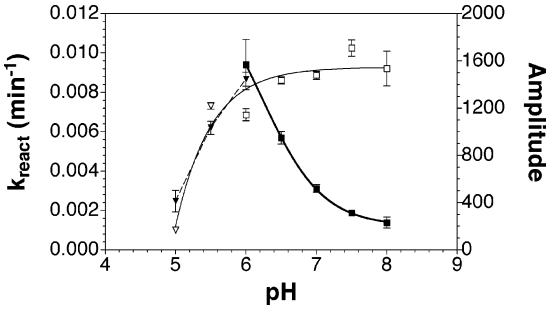

FIGURE 4: Effect of pH on the apparent rate constant (k_{react}) and amplitude for $KatG^N$ reactivation by $KatG^C$. $KatG^N$ and $KatG^C$ (1 μM each) were incubated together at 4 °C in 120 mM phosphate (squares) or 120 mM citrate (triangles) at various pHs. Aliquots were removed periodically to measure catalase activity at pH 7. From single exponential fits of the data, k_{react} values corresponding to rate (solid symbols) and amplitude values corresponding to maximum recovered activity (open symbols) were obtained. The bold solid line represents a fit of k_{react} (pH 6−8) to eq 1. The general trends of k_{react} (pH 6 and below) and amplitude (pH 5−8) are highlighted by the dashed and light solid lines, respectively. Catalase activity was measured in the presence of 8.5 mM H_2O_2 at 23 °C. The units for the amplitude are in reciprocal seconds because they are taken from rates of catalase activity divided by [$KatG^N$].

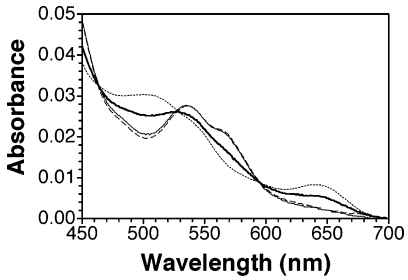

FIGURE 5: Effect of separately expressed and isolated $KatG^C$ on the visible absorption spectrum of $KatG^N$. A spectrum corresponding to the charge transfer and α and β transitions of the heme prosthetic group were recorded for $KatG^N$ alone (solid line), an equimolar mixture of $KatG^N$ and $KatG^C$ immediately after mixing (dashed line), and an equimolar mixture of $KatG^N$ and $KatG^C$ following a 48 h incubation at 4 °C (bold line). A typical spectrum for wtKatG is also shown (dotted line). Spectra were recorded in 100 mM phosphate buffer, pH 7.0, at 23 °C.

centration of $KatG^C$ to $KatG^N$ resulted in the appearance of EPR signals corresponding to high-spin pentacoordinate and hexacoordinate heme iron, as evident from a group of signals with *g*-values around 6 and increased amplitude near $g = 2$ (spectrum b); however, the hexacoordinate low-spin complex was still the dominant species present. Following a 48 h incubation (4 °C) of the two domains together, a dramatic increase in the high-spin species was observed along with the concomitant decrease in the hexacoordinate low-spin complex (spectrum c). Consistent with our UV−vis results,

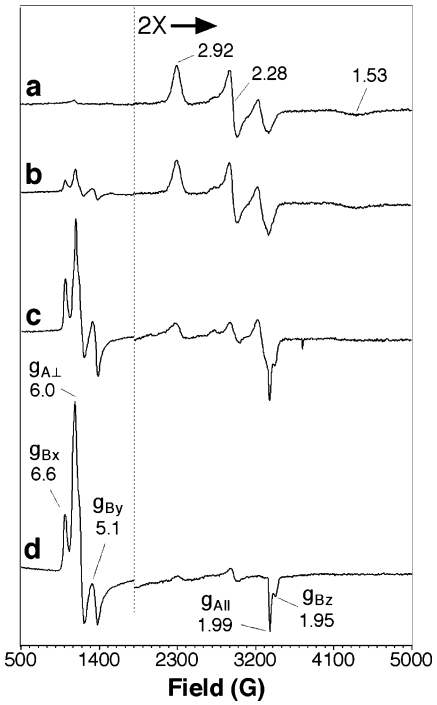

FIGURE 6: Effect of separately expressed and isolated $KatG^C$ on the EPR spectrum for $KatG^N$. An EPR spectrum was recorded for $KatG^N$ alone (a), $KatG^N$ immediately following mixture with equimolar $KatG^C$ (b), $KatG^N$ following a 48 h incubation (4 °C) with equimolar $KatG^C$ (c), and wtKatG (d). All spectra were recorded at 10 K. Spectrometer settings were as described in Materials and Methods. The *g*-values corresponding to the axial signal of the hexacoordinate high-spin ($A_\perp$ and $A_{||}$) and the rhombic signal of the pentacoordinate high-spin (B_x, B_y, and B_z) species are indicated in spectrum d.

some hexacoordinate low-spin complex was still observable after the 48 h incubation. However, the distribution of high-spin components in the spectrum bore a strong resemblance to that of wild-type KatG (compare signals at $g \sim 6$ in spectra c and d).

To investigate the discrepancy between restored $KatG^N$ active sites by activity (~20%) and by spectroscopy (~50%), we evaluated the effect of added H_2O_2 on the EPR spectrum of $KatG^N$ following its restructuring by $KatG^C$. H_2O_2 (20 equiv) was added and allowed to react for 1 h before the sample was frozen and a spectrum recorded. The signals corresponding to the pentacoordinate and hexacoordinate high-spin species were highly similar to the unreacted $KatG^N$/$KatG^C$ mixture. However, the signal intensity was diminished by roughly 30%. With the exception of a weak free radical signal at $g \sim 2$, no other obviously new species were detected (data not shown).

DISCUSSION

Despite its substantial distance from the active site and lack of any identifiable catalytic activity of its own, the C-terminal domain is clearly an integral component of catalase−peroxidase structure and catalysis. In the absence of the C-terminal domain, the N-terminal domain, which contains the active site, has no apparent activity. The active site heme is in a hexacoordinate low-spin state, and the strong field sixth ligand is likely supplied by the so-called distal histidine. Because heterolytic cleavage of hydroperoxide substrates requires their direct access to the heme iron, and because the distal histidine is required as a general base for the reaction, the loss of catalase and peroxidase activity is a reasonable expectation for active site rearrangement of this type.

These effects are at least partially reversed by the reintroduction of the C-terminal domain as a separate protein. The restructuring of the active site is evident, first of all, from spectroscopic analyses of the coordination environment of the heme. The UV−visible spectra clearly reveal an increase in high-spin heme species, and this comes at the expense of the hexacoordinate low-spin complex. The EPR spectra confirm these conclusions and also show a distribution between high-spin species nearly identical to that of the wild-type enzyme. The mixed population of coordination states for ferric catalase−peroxidases is a peculiarity of these enzymes, one that is highly sensitive to subtle changes around the active site induced by mutagenesis and, in some cases, aging, buffer conditions, etc. (*19*, *20*). It is striking that this distribution is so precisely reproduced by domain recombination.

The more exacting measure of active site reconstruction, however, is the presence of not only peroxidase activity but catalase activity as well. Recent studies by our laboratory and others indicate that the catalase activity of the catalase−peroxidases exists due to a precarious balance of factors. Precisely ordered hydrogen-bonding networks are required for catalase activity. These are either dependent upon (at least in part) or act in concert with a novel covalent cross-link between active site Trp 105, Tyr 226, and Met 252 (*E. coli* KatG numbering). Many catalase−peroxidase variants created by site-directed mutagenesis (*8*, *9*, *21*−*28*) and deletion mutagenesis (*2*) exhibit little or no catalase activity. Spectroscopic evaluation of these variants often indicates that only rather subtle modifications of the heme environment have resulted from these modifications (*2*, *8*, *9*, *21*−*26*). Indeed, the vast majority of these variants retain peroxidase activity equal to or better than their wild-type counterparts (*2*, *8*, *9*, *21*−*28*). The substantial catalase activity observed from $KatG^N$ upon incubation with $KatG^C$ indicates that the separate C-terminal domain supports a very precise restructuring of the active site environment.

Visual inspection of the reported catalase−peroxidase structures (*1*, *10*, *29*) and comparison to the known behavior of similar monofunctional peroxidases supports a connection between the presence or absence of the C-terminal domain and the coordination state of the heme iron, particularly as it involves the distal histidine (His 106). Prominent *intra*subunit interactions are observed between the B′C′ loop and E′ helix of the C-terminal domain and the BC loop of the N-terminal domain (Figure 7). Substantial *inter*subunit interactions are also observed between the AB loop and C helix of the N-terminal domain and a structure encompassing helices G′ through I′ of the C-terminal domain. On both sides of these interdomain interfaces, many of the individual residues involved in the interactions are strictly conserved across the catalase−peroxidases.

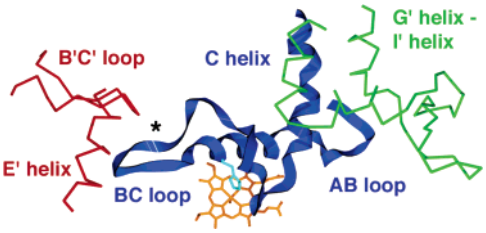

FIGURE 7: Interfaces between the N- and C-terminal domains of KatG. Structures from the N-terminal domain are shown as a blue ribbon. Structures from the *intra*subunit C-terminal domain are shown as red α-carbon traces. Structures from the *inter*subunit C-terminal domain are shown as green α-carbon traces. The heme (orange) and distal histidine (cyan) are also shown. All C-terminal domain structures are labeled with primed letters (e.g., B′C′ loop), and all structures from the N-terminal domain are shown with unaccented letters (e.g., AB loop). The approximate analgous location of the Ca^{2+} ion found in monofunctional peroxidases is indicated (*). Coordinates from the structure of *Burkholderia pseudomallei* KatG were used (PDB accession number 1MWV) (*10*).

Interestingly, many of the monofunctional peroxidases use a completely different strategy to support the BC loop and B helix. In the fungal secretory peroxidases (i.e., the class II peroxidases), a calcium ion is coordinated by residues from the BC loop and B helix (*30*, *31*). The loss of this calcium results in the coordination of the distal histidine to the heme iron, yielding a hexacoordinate low-spin heme in the active site and the concomitant loss of peroxidase activity (*32*−*34*). It is interesting to note that in our system k_{react} increases as pH decreases with an apparent pK_a of 6.2. This would be consistent with the protonation of a histidine residue to disfavor its coordination to the heme iron and thus achieve activation of $KatG^N$. Indeed, the bishistidine coordinated heme of Ca^{2+}-deficient manganese peroxidase (a class II peroxidase) loses a histidine ligand with decreasing pH according to a pK_a of 5.7 (*32*).

In the class III peroxidases (plant secretory peroxidases such as horseradish peroxidase and peanut peroxidase), the BC loop and B helix are further stabilized by a disulfide bond that straddles the calcium coordination site (*35*, 36). Thus, the loss of calcium by these enzymes produces a much less dramatic outcome. Less activity is lost, and a more subtle alteration of the heme environment occurs (*37*, *38*). Indeed, greater active site stability has been imparted to the class II manganese peroxidase (MnP) by using site-directed mutagenesis to introduce an analogous disulfide bond to that observed in the class III enzymes (*39*).

Among the class II and class III peroxidases, the shifts in heme coordination environment and loss of activity are reversible upon the reintroduction of calcium. Likewise, we demonstrate that the same consequences for structure and activity that are observed in catalase−peroxidase upon removal of the C-terminal domain can be reversed by reintroduction of the domain as a separately expressed and isolated protein.

The striking difference between these reactivation processes is the time course for active site restructuring.

Reintroduction of calcium to the class II and III peroxidases leads to rapid restoration of active site architecture and peroxidase activity. For example, incubation of inactivated MnP with calcium restores activity within a matter of minutes (*40*). Conversely, active site restructuring in $KatG^N$, as evident from shifts in heme coordination environment *and* catalytic activity, takes on the order of 24 h. This may be partially accounted for by the fact that reactivation of $KatG^N$ was accomplished with a single equivalent of $KatG^C$, whereas reactivation of MnP was carried out using over 30 equiv of Ca^{2+} (*40*). Nevertheless, to a first approximation, $KatG^N$ reactivation occurs at about one-tenth the rate of Ca^{2+}-dependent MnP reactivation.

This is suggestive of slow structural rearrangements that may precede the spectroscopic and catalytic evidence of reactivation. One possible process is the establishment of the Trp-Tyr-Met covalent adduct unique to catalase−peroxidases (*1*, *10*, *27*, *29*, *41*). However, this seems unlikely because establishment of the covalent adduct is peroxide dependent and occurs via formation of compound **I** (*8*, *26*). In our studies, no peroxide was added to induce activation, and compound **I** formation is not supported by the hexacoordinate low-spin complex observed in $KatG^N$. Thus, formation of the adduct could not precede the reorganization of the active site.

A second explanation is that structural perturbation of $KatG^N$ and/or $KatG^C$ is required to establish a productive conformation that allows for the subsequent restructuring of the active site. This would be consistent with the suggestion of Carpena et al. that the C-terminal domain serves as a platform to ensure the proper folding of the N-terminal domain (*42*). Indeed, there are several points of contact between the two domains, including those mentioned above. Although the precise sequence of events leading to active site restructuring remains to be established, our data suggest that large-scale unfolding and refolding of either domain at the secondary structural level are unlikely. Our $KatG^N$ and $KatG^C$ have CD spectra that are consistent with what is expected from the wild-type enzyme. The folded arrangement of $KatG^N$ is such that both active site histidines appear to serve as axial ligands to the heme iron (*11*). Importantly, there are no changes observed in CD upon coincubation of the separated domains. In any case, it is clear that $KatG^C$ is able to induce whatever structural changes in the N-terminal domain are necessary to restore its active conformation.

Interestingly, a rearrangement that involves shifts in preexistent structural elements could account for the observed data. All known catalase−peroxidase structures show an intricate association between the first 30 amino acids of both N-terminal domains. Each C-terminal domain also contributes to this part of the dimer interface (*1*, *10*, *29*). It is reasonable to suggest that, in the absence of the C-terminal domain, the first amino acids of the N-terminal domain adopt an alternative conformation that does not allow for the correct interaction across the dimer interface. It is anticipated that the switch out of such an alternative conformation could present a significant kinetic barrier to active site restructuring. Indeed, precedent for such slow conformational changes of exactly this type has been observed in the substrate-induced interconversion of quaternary isoforms of human porphobilinogen synthase. Rate constants for this interconversion as measured by substrate-induced reactivation of the enzyme were on the order of 1.7×10^{-2} min^{-1} (reported as 1.05 h^{-1}) (*43*), very similar to what we have observed for $KatG^N$ reactivation.

Whether measured spectroscopically (~50%) or by catalytic activity (~20%), active site restructuring by $KatG^N$ is not complete. It is possible that a fraction of the N-terminal domain is locked in a conformational state that is recalcitrant to the actions of $KatG^C$. We suggest that this is reported by the fraction that remains in its hexacoordinate low-spin state (~50%). At the present time, we have not identified conditions that address this population.

It also appears that although a proportion of $KatG^N$ is spectroscopically responsive to $KatG^C$-dependent restructuring, it either produces a less active conformation or produces a mixed population of active and inactive states. Two possible explanations are currently under investigation in our laboratory. One is that restructuring of $KatG^N$ by $KatG^C$ produces a proportion of active sites that, while spectroscopically similar to wild-type KatG, do not react correctly with H_2O_2. Indeed, the fact that reaction with a low concentration of H_2O_2 produces an appreciable change in EPR spectrum evident a full hour after addition suggests that at least some proportion of restructured $KatG^N$ is compromised with respect to catalytic consumption of the substrate.

A second and potentially related possibility is that some $KatG^N$ structural elements outside the active site are not arranged correctly by $KatG^C$ to yield full activity. Indeed, we have produced a $KatG^N$ variant lacking the so-called LL2 interhelical insertion.[2] This modified $KatG^N$ has no catalytic activity and forms a hexacoordinate low-spin complex just like $KatG^N$. Spectroscopically, the active site of this variant is restored to a similar extent (~50%) by equimolar $KatG^C$. However, unlike $KatG^N$, the peroxidase activity of this $KatG^N$ variant is restored to a commensurate level (≥50%) in comparison to the intact KatG lacking the same insertion.[3] Interestingly, an *inter*subunit point of contact between the domains occurs between the LL2 interhelical insertion of one subunit and the C-terminal domain of a second subunit. It is possible that $KatG^C$ does not fully or correctly address this structural feature in $KatG^N$.

In conclusion, the essential nature of the C-terminal domain to catalase−peroxidase structure and catalysis is demonstrated by its ability to restore, at least in part, the N-terminal domain to its bifunctionally active conformation. Reactivation of the enzyme in this manner provides a unique opportunity to probe the mechanisms by which the C-terminal domain directs the folding and maintenance of this uniquely bifunctional active site.

ACKNOWLEDGMENT

We are indebted to Dr. Holly Ellis for helpful discussions. We thank Dr. Evert Duin for assistance with EPR. DNA sequencing was carried out at the Davis Sequencing Facility by Eric Bowman, Carrie Stoltz, Michael Pollack, and Jaime Lizarraga.

[2] This interhelical insertion is known as large loop 2 (LL2) (*1*); it is also known as the FG insertion because it is located between the F and G helices of the N-terminal domain (*2*). KatG lacking this interhelical insertion has little or no catalase activity but retains substantial peroxidase activity (*2*).

[3] Y. Li and D. C. Goodwin, unpublished observations.

REFERENCES

1. Yamada, Y., Fujiwara, T., Sato, T., Igarashi, N., and Tanaka, N. (2002) The 2.0 Å crystal structure of catalase-peroxidase from *Haloarcula marismortui*, *Nat. Struct. Biol. 9*, 691−695.
2. Li, Y., and Goodwin, D. C. (2004) Vital roles of an interhelical insertion in catalase-peroxidase bifunctionality, *Biochem. Biophys. Res. Commun. 318*, 970−976.
3. Rattan, A., Kalia, A., and Ahmad, N. (1998) Multidrug-resistant *Mycobacterium tuberculosis*: molecular perspectives, *Emerging Infect. Dis. 4*, 195−209.
4. Brunder, W., Schmidt, H., and Karch, H. (1996) KatP, a novel catalase-peroxidase encoded by the large plasmid of enterohaemorrhagic *Escherichia coli* O157:H7, *Microbiology 142*, 3305−3315.
5. Garcia, E., Nedialkov, Y. A., Elliott, J., Motin, V. L., and Brubaker, R. R. (1999) Molecular characterization of KatY (antigen 5), a thermoregulated chromosomally encoded catalase-peroxidase of *Yersinia pestis*, *J. Bacteriol. 181*, 3114−3122.
6. Mehigh, R. J., and Brubaker, R. R. (1993) Major stable peptides of *Yersinia pestis* synthesized during the low-calcium response, *Infect. Immun. 61*, 13−22.
7. Chromy, B. A., Choi, M. W., Murphy, G. A., Gonzales, A. D., Corzett, C. H., Chang, B. C., Fitch, J. P., and McCutchen-Maloney, S. L. (2005) Proteomic characterization of *Yersinia pestis* virulence, *J. Bacteriol. 187*, 8172−8180.
8. Ghiladi, R. A., Medzihradszky, K. F., and Ortiz de Montellano, P. R. (2005) Role of the Met-Tyr-Trp cross-link in *Mycobacterium tuberculosis* catalase-peroxidase (KatG) as revealed by KatG(M255I), *Biochemistry 44*, 15093−15105.
9. Jakopitsch, C., Auer, M., Regelsberger, G., Jantschko, W., Furtmuller, P. G., Ruker, F., and Obinger, C. (2003) Distal site aspartate is essential in the catalase activity of catalase-peroxidases, *Biochemistry 42*, 5292−5300.
10. Carpena, X., Loprasert, S., Mongkolsuk, S., Switala, J., Loewen, P. C., and Fita, I. (2003) Catalase-peroxidase KatG of *Burkholderia pseudomallei* at 1.7 Å resolution, *J. Mol. Biol. 327*, 475−489.
11. Baker, R. D., Cook, C. O., and Goodwin, D. C. (2004) Properties of catalase-peroxidase lacking its C-terminal domain, *Biochem. Biophys. Res. Commun. 320*, 833−839.
12. Scott, S. L., Chen, W.-J., Bakac, A., and Espenson, J. H. (1993) Spectroscopic parameters, electrode potentials, acid ionization constants, and electron exchange rates of the 2,2′-azinobis(3-ethylbenzthiazoline-6-sulfonate) radicals and ions, *J. Phys. Chem. 97*, 6710−6714.
13. Nelson, D. P., and Kiesow, L. A. (1972) Enthalpy of decomposition of hydrogen peroxide by catalase at 25 °C (with molar extinction coefficients of H_2O_2 solutions in the UV), *Anal. Biochem. 49*, 474−478.
14. Gill, S. C., and von Hippel, P. H. (1989) Calculation of protein extinction coefficients from amino acid sequence data, *Anal. Biochem. 182*, 319−326.
15. Varnado, C. L., Hertwig, K. M., Thomas, R., Roberts, J. K., and Goodwin, D. C. (2004) Properties of a novel periplasmic catalase-peroxidase from *Escherichia coli* O157:H7, *Arch. Biochem. Biophys. 421*, 166−174.
16. Claiborne, A., and Fridovich, I. (1979) Purification of the *o*-dianisidine peroxidase from *Escherichia coli* B. Physicochemical characterization and analysis of its dual catalatic and peroxidatic activities, *J. Biol. Chem. 254*, 4245−4252.
17. Gadsby, P. M. A., and Thomson, A. J. (1990) Assignment of the axial ligands of ferric ion in low-spin hemoproteins by near-infrared magnetic circular dichroism and electron paramagnetic resonance spectroscopy, *J. Am. Chem. Soc. 112*, 5003−5011.
18. Palmer, G. (1979) Electron paramagnetic resonance of hemoproteins, in *The porphyrins: physical chemistry, part B* (Dolphin, D., Ed.) pp 313−350, Academic Press, New York.
19. Chouchane, S., Girotto, S., Kapetanaki, S., Schelvis, J. P., Yu, S., and Magliozzo, R. S. (2003) Analysis of heme structural heterogeneity in *Mycobacterium tuberculosis* catalase-peroxidase (KatG), *J. Biol. Chem. 278*, 8154−8162.
20. Jakopitsch, C., Ivancich, A., Schmuckenschlager, F., Wanasinghe, A., Poltl, G., Furtmuller, P. G., Ruker, F., and Obinger, C. (2004) Influence of the unusual covalent adduct on the kinetics and formation of radical intermediates in synechocystis catalase peroxidase: a stopped-flow and EPR characterization of the MET275, TYR249, and ARG439 variants, *J. Biol. Chem. 279*, 46082−46095.
21. Hillar, A., Peters, B., Pauls, R., Loboda, A., Zhang, H., Mauk, A. G., and Loewen, P. C. (2000) Modulation of the activities of catalase-peroxidase HPI of *Escherichia coli* by site-directed mutagenesis, *Biochemistry 39*, 5868−5875.
22. Jakopitsch, C., Auer, M., Regelsberger, G., Jantschko, W., Furtmuller, P. G., Ruker, F., and Obinger, C. (2003) The catalytic role of the distal site asparagine-histidine couple in catalase-peroxidases, *Eur. J. Biochem. 270*, 1006−1013.
23. Jakopitsch, C., Auer, M., Ivancich, A., Ruker, F., Furtmuller, P. G., and Obinger, C. (2003) Total conversion of bifunctional catalase-peroxidase (KatG) to monofunctional peroxidase by exchange of a conserved distal side tyrosine, *J. Biol. Chem. 278*, 20185−20191.
24. Yu, S., Girotto, S., Zhao, X., and Magliozzo, R. S. (2003) Rapid formation of compound II and a tyrosyl radical in the Y229F mutant of *Mycobacterium tuberculosis* catalase-peroxidase disrupts catalase but not peroxidase function, *J. Biol. Chem. 278*, 44121−44127.
25. Regelsberger, G., Jakopitsch, C., Ruker, F., Krois, D., Peschek, G. A., and Obinger, C. (2000) Effect of distal cavity mutations on the formation of compound I in catalase-peroxidases, *J. Biol. Chem. 275*, 22854−22861.
26. Ghiladi, R. A., Knudsen, G. M., Medzihradszky, K. F., and Ortiz de Montellano, P. R. (2005) The Met-Tyr-Trp cross-link in *Mycobacterium tuberculosis* catalase-peroxidase (KatG): autocatalytic formation and effect on enzyme catalysis and spectroscopic properties, *J. Biol. Chem. 280*, 22651−22663.
27. Donald, L. J., Krokhin, O. V., Duckworth, H. W., Wiseman, B., Deemagarn, T., Singh, R., Switala, J., Carpena, X., Fita, I., and Loewen, P. C. (2003) Characterization of the catalase-peroxidase KatG from Burkholderia pseudomallei by mass spectrometry, *J. Biol. Chem. 278*, 35687−35692.
28. Eady, N. A. J., Jesmin, N. A. J., Servos, S., Cass, A. E. G., Nagy, J. M., and Brown, K. A. (2005) Probing the function of *Mycobacterium tuberculosis* catalase-peroxidase by site-directed mutagenesis, *Dalton Trans. 2005*, 3495−3500.
29. Bertrand, T., Eady, N. A., Jones, J. N., Jesmin, Nagy, J. M., Jamart-Gregoire, B., Raven, E. L., and Brown, K. A. (2004) Crystal structure of *Mycobacterium tuberculosis* catalase-peroxidase, *J. Biol. Chem. 279*, 38991−38999.
30. Poulos, T. L., Edwards, S. L., Wariishi, H., and Gold, M. H. (1993) Crystallographic refinement of lignin peroxidase at 2 Å, *J. Biol. Chem. 268*, 4429−4440.
31. Sundaramoorthy, M., Kishi, K., Gold, M. H., and Poulos, T. L. (1994) The crystal structure of manganese peroxidase from *Phanerochaete chrysosporium* at 2.06-Å resolution, *J. Biol. Chem. 269*, 32759−32767.
32. Sutherland, G. R., Zapanta, L. S., Tien, M., and Aust, S. D. (1997) Role of calcium in maintaining the heme environment of manganese peroxidase, *Biochemistry 36*, 3654−3662.
33. Nie, G., and Aust, S. D. (1997) Spectral changes of lignin peroxidase during reversible inactivation, *Biochemistry 36*, 5113−5119.
34. Nie, G., and Aust, S. D. (1997) Effect of calcium on the reversible thermal inactivation of lignin peroxidase, *Arch. Biochem. Biophys. 337*, 225−231.
35. Schuller, D. J., Ban, N., Huystee, R. B., McPherson, A., and Poulos, T. L. (1996) The crystal structure of peanut peroxidase, *Structure 4*, 311−321.
36. Gajhede, M., Schuller, D. J., Henriksen, A., Smith, A. T., and Poulos, T. L. (1997) Crystal structure of horseradish peroxidase C at 2.15 Å resolution, *Nat. Struct. Biol. 4*, 1032−1038.
37. Shiro, Y., Kurono, M., and Morishima, I. (1986) Presence of endogenous calcium ion and its functional and structural regulation in horseradish peroxidase, *J. Biol. Chem. 261*, 9382−9390.
38. van Huystee, R. B., Xu, Y., and O'Donnell, J. P. (1992) Variation in Soret absorptions of peroxidase due to calcium, *Plant Physiol. Biochem. 30*, 293−297.
39. Reading, N. S., and Aust, S. D. (2000) Engineering a disulfide bond in recombinant manganese peroxidase results in increased thermostability, *Biotechnol. Prog. 16*, 326−333.
40. Sutherland, G. R., and Aust, S. D. (1997) Thermodynamics of binding of the distal calcium to manganese peroxidase, *Biochemistry 36*, 8567−8573.
41. Jakopitsch, C., Kolarich, D., Petutschnig, G., Furtmuller, P. G., and Obinger, C. (2003) Distal side tryptophan, tyrosine and

methionine in catalase-peroxidases are covalently linked in solution, *FEBS Lett. 552*, 135−140.
42. Carpena, X., Melik-Adamyan, W., Loewen, P. C., and Fita, I. (2004) Structure of the C-terminal domain of the catalaseperoxidase KatG from *Escherichia coli*, *Acta Crystallogr., Sect. D: Biol. Crystallogr. 60*, 1824−1832.
43. Tang, L., Stith, L., and Jaffe, E. K. (2005) Substrate-induced interconversion of protein quaternary structure isoforms, *J. Biol. Chem. 280*, 15786−15793.

BI052392Y